Earth Systems and Environment
https://doi.org/10.1007/s41748-024-00474-1

ORIGINAL ARTICLE

The Impact of Urban Particulate Matter on Lightning Frequency in Thunderstorms: A Case Study of the Bangkok Metropolitan Region

Jojinda Sae-Jung[1] · Mace Bentley[2] · Tobias Gerken[2] · Zhuojun Duan[3]

Received: 10 June 2024 / Revised: 20 August 2024 / Accepted: 15 September 2024

Abstract
Bangkok, Thailand is a tropical Asian megacity with high aerosol concentrations and frequent thunderstorm activity. This investigation examines the covariation between thermodynamics, aerosols, and thunderstorms, using lightning stroke counts as a measure of intensity, for a five-year period (2016–2020). The investigation incorporates data from the aerosol robotic network (AERONET), ERA-5 reanalysis, ground-based air quality stations, and total lighting data from Vaisala Inc.'s GLD360 network to examine the aerosol-thermodynamic interrelationships within thunderstorm initiation environments. Results indicate that aerosol impacts on thunderstorms are robust and, when examined in concert with instability, can augment lightning. Thermodynamic instability is also positively correlated with stroke counts in thunderstorms. Particulate matter greater than 10 μg m^{-3} (PM10) concentration is significantly higher in thunderstorms containing more than 100 strokes, supporting the potential role of aerosols in promoting the non-inductive charge process. The emergence of a "boomerang" or threshold effect is also evident as aerosol optical depth (AOD) increases. Evidence suggests increasing AOD initially promotes, then limits, instability and thunderstorm intensity. Finally, there exists a positive relationship between aerosol concentration and particle size in thunderstorm initiation environments.

Keywords Aerosols · Air pollution · Lightning frequency · Particulate matter · Thermodynamic instability · Thunderstorm intensity

1 Introduction and Background

Recognizing how thermodynamic and aerosol processes act to promote atmospheric convection is vital for understanding climate change (Fan et al. 2013; Li et al. 2017). Although feedbacks between thermodynamics and aerosols have been examined at multiple scales, the extent of their integration remains poorly understood (Sun et al. 2023). Evidence suggests, lightning activity in urban thunderstorms is sensitive to both thermodynamics and aerosol concentrations due to greater atmospheric instability being required to overcome increases in aerosol loads. Therefore, when both elevated instability and aerosol concentrations are present, as in urban areas, lightning production appears maximized (Bentley et al. 2024). Numerical modeling has simulated these relationships across idealized conditions (van den Heever et al. 2006; Ekman et al. 2011; Fan et al. 2013; Schmid and Niyogi 2017; Sun et al. 2023); however, there exists few observational investigations examining lightning variability across a range of urban atmospheric conditions (Dewan et al. 2024; Bentley et al. 2024).

We conduct a multi-variable analysis of urban thunderstorm environments in the Bangkok Metropolitan Region (BMR). A central premise of this investigation is that although isolating thermodynamic and aerosol mechanisms may be useful in terms of simplifying a description of their causality, it overlooks the importance of their mutual integration (Williams et al. 2002, 2004; Carrio and Cotton 2011). Therefore, data mining is utilized to analyze the covariance of thermodynamic instability, aerosols, and thunderstorm intensity, as measured

✉ Mace Bentley
bentleml@jmu.edu

1 Geography Program, Faculty of Liberal Arts, Thammasat University, Bangkok, Thailand

2 School of Integrated Sciences, James Madison University, Harrisonburg, VA, USA

3 Department of Computer Science, James Madison University, Harrisonburg, VA, USA

Published online: 26 September 2024

by lightning stroke counts. The coupling of thermodynamic and aerosol processes is evaluated in time and space over a range of environments in order to provide useful insights for atmospheric scientists, urban planners, and hazards scholars.

It is estimated that more than two-thirds of the global population will reside in cities by 2050 (Yair 2018). In Asia, the "threshold urban size" has been exceeded in many cities where deleterious impacts of urbanization have accelerated environmental change (Yair 2018). Bangkok, Thailand continues to undergo rapid urbanization. In fact, aside from the Chinese Pearl River Delta, the BMR is one of the most extensively developed areas within Asia (Small et al. 2018). One result of BMR urbanization is a per capita area of green space of only 3.3 m^2, versus a regional average of 38.6 m^2 (Small et al. 2018). This lack of green space has led to an increase in urban heat, especially along development corridors emanating from the urban core (Bentley et al. 2020; Arfanuzzaman and Dahiya 2019; Arifwidodo and Tanaka 2015). The elevated land surface temperatures intensify the urban heat island (UHI) (Oke 1982; Voogt and Oke 2003; Bentley et al. 2020). Similar to other low latitude cities, the size and intensity of the BMR UHI appears to be an important variable shaping the local and regional lightning and thunderstorm distribution (Naccarato et al. 2003; Stallins et al. 2006; Morales Rodriguez et al. 2010; Bentley et al. 2020; Sae-Jung et al. 2024). The combined effects of the UHI and atmospheric pollution within the BMR create a conducive environment for storm electrification and subsequent thunderstorm augmentation through increasing thermodynamic instability and urban particulate matter. The varying sizes and concentration of anthropogenically sourced aerosols include cloud condensation nuclei (CCN) that can significantly modify cloud development (Fan et al. 2007; van den Heever and Cotton 2007; Wang et al. 2011). Anthropogenically sourced aerosols can also modulate cloud growth, alter cloud microphysics, warm rain production, and the generation of lightning (Rosenfeld and Lensky 1998; Konwar et al. 2012; Rosenfeld et al. 2016; Zhu et al. 2014, 2015; Guo et al. 2018; Huang et al. 2022; Bentley et al. 2024).

Variables assessing moisture, temperature, and thermodynamics are often used in thunderstorm prediction (Craven and Brooks 2004; Williams et al. 2005; Wang et al. 2009). Atmospheric aerosol loads (i.e., particulate matter) also impact atmospheric convection and cloud electrification (Andreae et al. 2004; Khain et al. 2005, 2008; van den Heever et al. 2011; Tao et al. 2007, 2012; Rosenfeld et al. 2008, 2014; Altaratz et al. 2014; Li et al. 2017; Wang et al. 2023; Bentley et al. 2024; Dewan et al. 2024). When the mixed-layer atmosphere has a higher aerosol content, as exists in polluted, urban air, more numerous cloud droplets efficiently transport water above the freezing level. Different states of water within the developing cloud act to separate electrical charges and accelerate lightning production (Reynolds et al. 1957). At temperatures below − 15 °C, graupel and snow crystals develop opposing charges. The accumulation of negatively charged graupel in the middle of the cloud versus positively charged ice crystals near the top promotes electrification and lightning production (Reynolds et al. 1957). Latent heat release generated by condensation and freezing within the cloud enhances the vertical motion field (Khain et al. 2005; Rosenfeld et al. 2008; Li et al. 2017; Sun et al. 2023). Increased convective available potential energy (CAPE) from urban heat also facilitates the vertical transport of water droplets above the freezing level, enhancing charge separation and flash production (Steiger and Orville 2003). These mechanisms of storm electrification are collectively known as the non-inductive charge separation process (MacGorman and Rust 1998; Seity et al. 2003).

Cleaner air has the opposite effect on cloud electrification, diminishing lightning since water is shared among fewer CCN and cloud droplets (Sun et al. 2023). Less polluted environments also exhibit early rainout and weaker vertical transport into the mixed phase region producing less lightning (Rosenfeld et al. 2008). Evidence suggests that convective processes accelerating cloud electrification may occur up to a given threshold of particulate matter and then decrease, as higher particulate concentrations partition sunlight and stabilize the atmosphere (Rosenfeld et al. 2002, 2008; van den Heever and Cotton 2007; Fuchs et al. 2015; Bentley et al. 2024). High concentrations of particulate matter can also act to warm the atmosphere, reducing relative humidity and stabilizing lapse rates. The conditions leading to an initial increase, and subsequent decrease in lightning activity are collectively known as the "boomerang effect" (Koren et al. 2008; Altaratz et al. 2010; Li et al. 2017).

By analyzing thunderstorm initiation environments and intensity with respect to total lightning frequency, we examine the aerosol-thermodynamic interrelationships of the BMR, an Asian megacity that exhibits complex controls on the regional lighting and thunderstorm distribution (Bentley et al. 2021; Sae-Jung et al. 2024). We evaluate a large dataset of thunderstorm events based on lightning characteristics and incorporate hourly aerosol and meteorological data. We examine how variations in thermodynamic instability, particulate matter, and thunderstorm intensity covary across the BMR utilizing data mining techniques. This is one of the first investigations of urban thunderstorms to assemble and statistically evaluate a large database of observational variables useful in assessing relationships between thermodynamic instability, pollution, and lightning frequency (Bentley et al. 2024). It is also the first study to examine relationships between thermodynamic instability, aerosols, and thunderstorm intensity in the BMR.

2 Study Region

The BMR, defined for this investigation and in prior research evaluating the UHI and thunderstorm climatology, is 6,400 km^2 and includes the Bangkok Metropolis, a 1,568 km^2 area also known as the Bangkok Metropolitan Area (Bentley et al. 2020, 2021; Sae-Jung et al. 2024; Fig. 1). This region encompasses the primary areas of urbanization and urban development corridors in the Chao Phraya River Delta (Bentley et al. 2020). The BMR is also located within the Chao Phraya River flood plain and has a growing population exceeding 11 million.

The BMR's climate is classified as a tropical savannah climate (Kottek et al. 2006). The BMR's monthly temperatures exceed 18 °C all year and there exists a pronounced dry season of less than 60 mm in a month. Bangkok's average annual rainfall is 1,450 mm. The months with the highest and least amount of rainfall are September (320 mm) and January (10.2 mm), respectively. There is an annual average of 137 rainy days, with September (22 days) and January (2 days) having the most and the least rain days, respectively.

3 Data and Methods

Five years (2016–2020) of GLD360 total lightning stroke data are used to construct a thunderstorm database and identify thunderstorm initiation environments. The GLD360 is a ground-based lightning location system owned and operated by Vaisala, Inc. (Said et al. 2010; Poelman et al. 2013; Mallick et al. 2014). Instruments in the GLD360 global network detect radio atmospherics emanating from lightning strokes. Polarity and peak current of each stroke are determined by evaluating lightning waveforms and applying an attenuation model. Each sensor determines time of arrival and employs a magnetic direction finder technology to spatiotemporally locate lightning strokes. Cloud-to-ground versus in-cloud lightning strokes are not determined in the GLD360 data; therefore, the system detects and archives in-cloud and ground stroke lightning activity (Holle and Murphy 2017).

On 18 August, 2015, Vaisala, Inc. upgraded the GLD360 network (Said and Murphy 2016). Ground and in-cloud lightning stroke detection efficiencies improved from 55 to 75% to 75–85% and from 10 to 30% to 40–50%, respectively. Median locational accuracy also increased from 2.4 km to 1.8 km (Said and Murphy 2016). Given the significant improvements to the network in detection efficiency and spatial resolution, this investigation utilizes lightning stroke data beginning in 2016. Uniform detection efficiency is expected across the

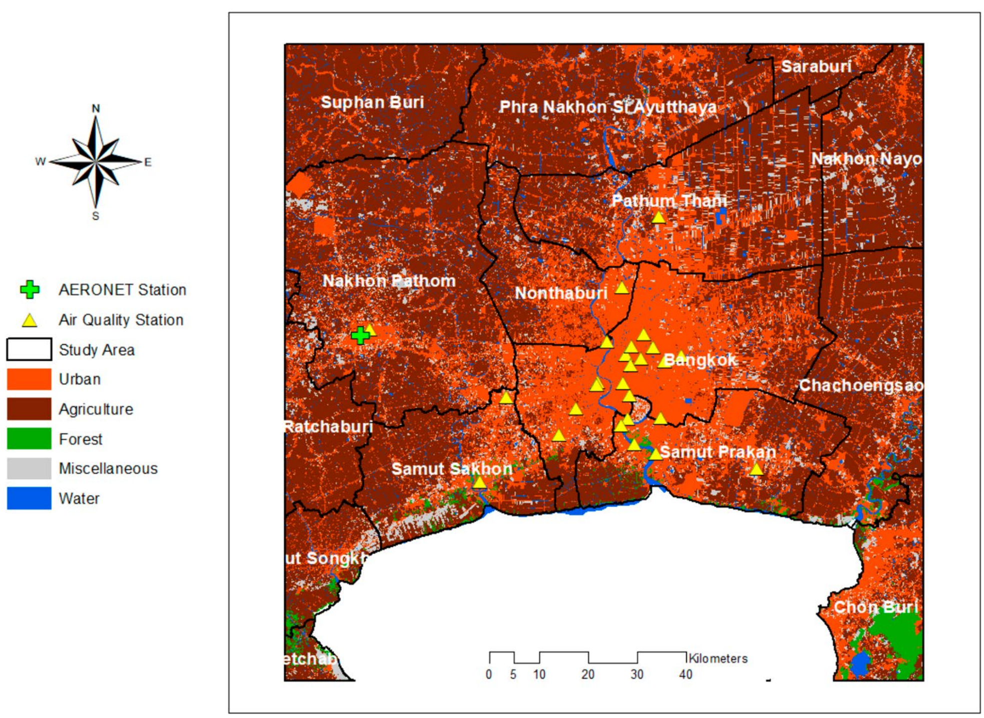

Fig. 1 Bangkok Metropolitan Region study area and 2019–2023 reclassified land use from the Land Development Department, the Ministry for Agriculture and Cooperatives, Thailand. Out of the 17 provinces in the study region, one had 2023 land use data, ten had 2021 land use data, three had 2020 land use data, and three had 2019 land use data. Location of the AERONET site at Silapakorn University in Nakhon Pathom province as well as the 26 stations maintained and operated by the Pollution Control Department, Ministry of Natural Resource and Environment, Royal Thai Government are shown

BMR given its comparative size within the global lightning network (Holle et al. 2017).

To identify thunderstorms from the 5,411,026 strokes detected in the BMR, a thunderstorm tracking algorithm was created that evaluates the spatial and temporal clustering of lightning (Sae-Jung et al. 2024). The identification of thunderstorms using lightning data are possible since a focused area of lightning occurs along a thunderstorm's path (see Sae-Jung et al. (2024) for more details on the thunderstorm tracking algorithm). During days with frequent thunderstorms, the thunderstorm detection algorithm can combine outflow-initiated thunderstorms with prior storms if their lightning strokes occur within the predefined temporal and spatial bounds of 15 min and 15 km (Sae-Jung et al. 2024). Therefore, the 52,608 thunderstorms identified by the algorithm are denoted as thunderstorm events (hereafter, TEs; Sae-Jung et al. 2024). By defining the TE track using a line segment from the initial to the last lightning stroke, path length, direction of movement, and TE density are discernible (Sae-Jung et al. 2024). Hourly aerosol and ECMWF ERA5 gridded data were then incorporated with TEs by determining the time and location of the first stroke in each TE and incorporating the most proximal measurement from the hourly aerosol and gridded datasets.

The ECMWF ERA5 hourly, 30 km gridded dataset was used to extract wind direction, wind speed, and CAPE for the initiation time and location of each TE. ERA5 is produced using 4D-Var data assimilation and model forecasts in CY41R2 of the ECMWF Integrated Forecast System (IFS; Hersbach et al. 2020). The transport wind is one of the most important meteorological variables for determining the dilution of air pollutants over urban areas (Miller 1967).

Hourly, level 2.0 ground-based radiometer data from the AErosol RObotic NETwork (AERONET) site at Silapakorn University in Nakhon Pathom province were used to obtain the spectral, 500 nm aerosol optical depth (AOD, a dimensionless measure of particle concentration) and 675 –440 nm Angstrom exponent (AE, a dimensionless measure related to particle size distribution; Fig. 1). AERONET Level 2.0 data have been comprehensively quality-controlled for cloud contamination and are cross-correlated with satellite-based estimates of AOD (Green et al. 2009; Li et al. 2009). The AOD-AE scatter plot is a useful graph to classify aerosol types (Morales Rodriguez et al. 2010).

Hourly measurements of particulate matter with diameters that are equal or less than 10 micrometers (PM10) and particulate matter with diameters that are equal or less than 2.5 micrometers (PM2.5) from 26 stations maintained and operated by the Pollution Control Department, Ministry of Natural Resource and Environment, Royal Thai Government, were used to assess particulate matter concentration (Fig. 1). The nearest station (in time and distance) corresponding to TE initiation was chosen for the PM10 and PM2.5 measurements. The PM10 or PM2.5 measurement was denoted as missing if more than 3 h elapsed between TE initiation and the closest measuring station. After removing TEs due to missing PM data, 15,928 events were available for further analyses. The mean time and distance from TE initiation locations to the closest PM measurement were 16 min and 38.6 km, respectively. This spatiotemporal adjacency of PM measurements to TE initiation is similar to prior investigations examining proximity environments of thunderstorms (30 min, 40 km; Thompson et al. 2003). Additionally, sensitivity tests were conducted that varied the distance between the closest PM station and TE initiation location from 5 km to 30 km. Although the sample size of TEs were reduced when lowering the distance to PM station, no significant differences in the PM25/PM10 mean values and distributions were found in comparison to the original criteria.

Prior research suggests, PM10 and PM2.5 are useful measures for estimating aerosols in thunderstorm environments when accounting for CAPE (Li et al. 2017; Wang et al. 2018; Bentley et al. 2024). It is useful to examine PM2.5 and PM10 separately since they vary independently in the BMR across the wet and dry seasons (Narita et al. 2019). During the wet season, PM10 remains relatively stable at nearly 80% of the dry season amount, while PM2.5 is much lower, at around half of the dry season concentration (Narita et al. 2019).

Relationships between CAPE and aerosol quantities (AOD, PM2.5, and PM10) were analyzed by stratifying the data into quantiles (Table 1). This categorization ensures enough TEs for statistical analysis in all quantile bins, including more extreme thermodynamic and aerosol environments (i.e., 75th to 90th and > 90th percentiles).

Table 1 Quantile statistics of PM2.5, PM10, AOD, CAPE, and flashes per event for the BMR

	0.25	0.5	0.75	0.9	0.95	1
CAPE ($J\ kg^{-1}$)	672	1087	1599	2172	2552	4978
PM2.5 ($\mu g\ m^{-3}$)	9	14	21	30	38	105
PM10 ($\mu g\ m^{-3}$)	19	27	38	51	59	154
AOD 500 nm (-)	0.20	0.34	0.54	0.77	1.08	2.22
Flashes $event^{-1}$	2	8	73	299	550	5568

It is important to note that our investigation examines the relationship of thunderstorm stroke counts, a measure of thunderstorm intensity, as a function of PM2.5, PM10, AOD, and CAPE (Bentley et al. 2024). The class averages for all quantities as well as their confidence intervals (5th – 95th percentile) were calculated. Confidence intervals were generated using $n = 1000$ bootstrapped samples (James et al. 2017).

Statistical significance testing utilized three methods to assess relationships at the 95% confidence level: analysis of variance (ANOVA; t-test), difference of medians (Kruskal-Wallis), and difference of distributions (Kolmogorov-Smirnov). An analysis of variance (ANOVA) test is a parametric testing method that indicates whether the mean varies across multiple categories (Karson et al. 1968). A Kruskal-Wallis test is a non-parametric testing method that indicates whether values tend to differ across multiple categories (Kruskal and Wallis 1952). If the values are drawn from distributions having the same geometric shape but different locations, the Kruskal-Wallis test can be interpreted as a test of whether the group medians are equal. A Kolmogorov-Smirnov test is a non-parametric testing method that indicates whether values tend to have different distributions across categories (Karson et al. 1968). Unlike an ANOVA test, it evaluates differences in distribution and mean; however, the Kolmogorov-Smirnov test requires more observations than other tests to detect differences.

3.1 Study Limitations

Although surface PM concentrations are not necessarily representative of the particle distribution available throughout the atmospheric column, measurements of particulate matter in thunderstorm initiation environments appear helpful for evaluating aerosol relationships with convective processes (Stallins et al. 2013; Yair et al. 2022; Perez-Invernon et al. 2023; Bentley et al. 2024). Given the importance of spatiotemporal proximity when evaluating relationships with respect to TE initiation, the measurements from the air quality stations and AERONET site may lack the resolution to examine the in-cloud environments of the ice-phase microphysics during thunderstorm lifecycles. Therefore, we extract large sample sizes of TEs (52,608 with AERONET/ERA5 data and 15,928 with AERONET/ERA5/PM data) across a wide range of aerosol and thermodynamic conditions. By evaluating TE intensity and interrelationships with aerosols and thermodynamics in the BMR, our goal is to evaluate the range of urban atmospheric environments occurring in thunderstorms. Through assessing urban thunderstorm variability, examining relationships between urban particulate matter and thermodynamics, and determining the role of urban areas in augmenting thunderstorm activity, our goal is to advance the understanding of urban weather environments and thunderstorm intensity.

4 Results

The relationship between thermodynamic instability and thunderstorm intensity is well documented (Williams et al. 2002; Pawar et al. 2012; Murugavel et al. 2014; Dewan et al. 2018; Sun et al. 2023; Wang et al. 2023; Bentley et al. 2024). There exists a statistically significant, positive relationship in means, medians, and overall distributions between CAPE and TE flash counts in the BMR (Fig. 2). This relationship exhibits narrow 95% confidence intervals for TE flash counts ranging from 1,125 J kg^{-1} for TEs with less than 10 strokes to 1,827 J kg^{-1} for TEs producing greater than 1,000 strokes (Fig. 2). 11% of TEs with less than 10 strokes (2,962 out of 27,078 TEs) occurred with CAPE greater than 2,000 J kg^{-1}, in comparison to

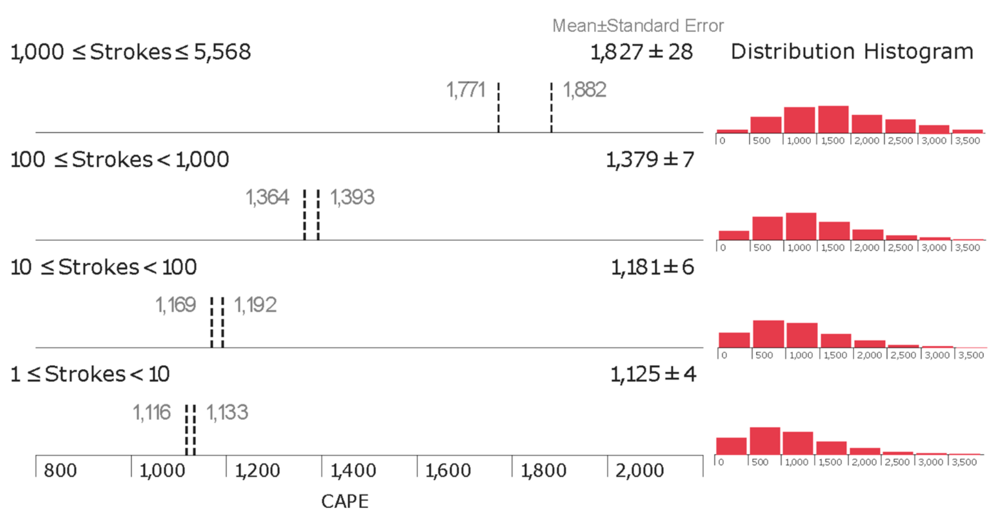

Fig. 2 Distribution plot of CAPE mean values +/- standard error and 95% confidence interval ranges across TE stroke count categories. Bar charts of the TE distribution in each stroke category are illustrated

the 37% of TEs with more than 1,000 strokes (340 out of 912 TEs; Fig. 2). The positive relationship between CAPE and lightning appears significant across global thunderstorm environments, regardless of geographical location and/or climate type (Bentley et al. 2024). Given the ability of thermodynamic instability to modulate thunderstorm intensity and stroke counts, the TEs will be stratified by CAPE when examining aerosol impacts.

Evidence of the "boomerang effect" is apparent when examining the relationship between CAPE and PM2.5 within TE initiation environments (Koren et al. 2008; Fig. 3). When stratifying the data by PM2.5 quantiles, CAPE increases until PM2.5 reaches the 75th percentile (21 μg m^{-3}), after which it appears to be suppressed, possibly due to a shifting importance from microphysical to radiative effects of cloud aerosols (Wang et al. 2018; Fig. 3). CAPE is maximized, with a mean of 1,378 J kg^{-1}, for TEs initiating in PM2.5 environments between the 50th and 75th quantile (14 to 21 μg m^{-3}; Fig. 3). For TE environments with PM2.5 between the 50th and 75th, 75th and 90th, and greater than the 90th quantiles, statistically significant differences in the mean, median, and distribution of CAPE were found as instability decreases under PM2.5 amounts greater than the 75th quantile (21 μg m^{-3}; Fig. 3). Focusing on TEs with greater than 1,000 strokes (912 TEs), a similar boomerang shape of the CAPE distribution with respect to PM2.5 quantiles is evident (not shown). Although not statistically significant at the 95% confidence level due to the smaller sample size, CAPE is once again maximized in TEs with greater than 1,000 strokes, between the 50th and 75th PM2.5 quantile (14 to 21 μg m^{-3}).

In contrast to the PM2.5 and CAPE relationship, there exists is a statistically significant, positive correlation in the mean, median, and distribution of PM2.5 across all stroke count categories within TEs (Fig. 4). A significant increase in mean PM2.5 occurs in TEs with greater than 1,000 strokes in comparison to the other stroke categories (Fig. 4). When examining TEs initiating in the 90th quantile of PM2.5 (> 30 μg m^{-3}), 29% were events greater than 1,000 strokes (44 of 154 TEs), while only 9% (636 of 7,070 TEs) were events with less than 10 strokes (Fig. 4). Eight TEs with greater than 1,000 strokes occurred in initiation environments containing PM2.5 of 55 μg m^{-3}, illustrated in the rightward shift of the distribution bar graphs across stroke categories (Fig. 4). When examining mean stroke counts across PM2.5 quantiles, TEs with PM2.5 less than the 25th quantile (2,995 events; < 9 μg m^{-3}) and above the 90th quantile (1,394 events; > 30 μg m^{-3}) produced a mean of 54 and 140 strokes TE^{-1}, respectively.

The distribution of CAPE across PM10 quantiles differs from PM2.5 in that there is no apparent suppression of CAPE as PM10 increases (Figs. 3 and 5). Only 55% of TEs (896 of 1,642 TEs) initiating in environments with PM10 greater than the 90th quantile (> 51 μg m^{-3}), also recorded PM2.5 greater than the 90th quantile (> 30 μg m^{-3}). There exists a statistically significant, positive relationship in the mean, median, and distribution between PM10 and CAPE across all quantiles. 20% of TEs (326 of 1,642 TEs) initiating in environments with PM10 greater than the 90th quantile (> 51 μg m^{-3}), recorded CAPE greater than or equal to 2,000 J kg^{-1}. This compares to only 7% of TEs (253 of 3,844 TEs) with CAPE greater

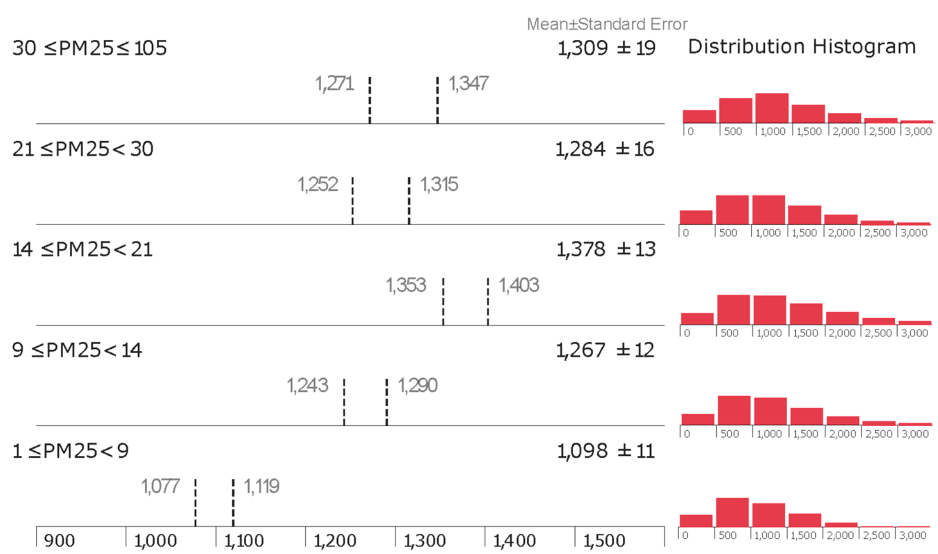

Fig. 3 Distribution of CAPE mean values +/-standard error and 95% confidence interval ranges across PM2.5 quantiles (25th, 50th, 75th, 90th). Bar charts of the TE distribution in each PM2.5 quantile are illustrated

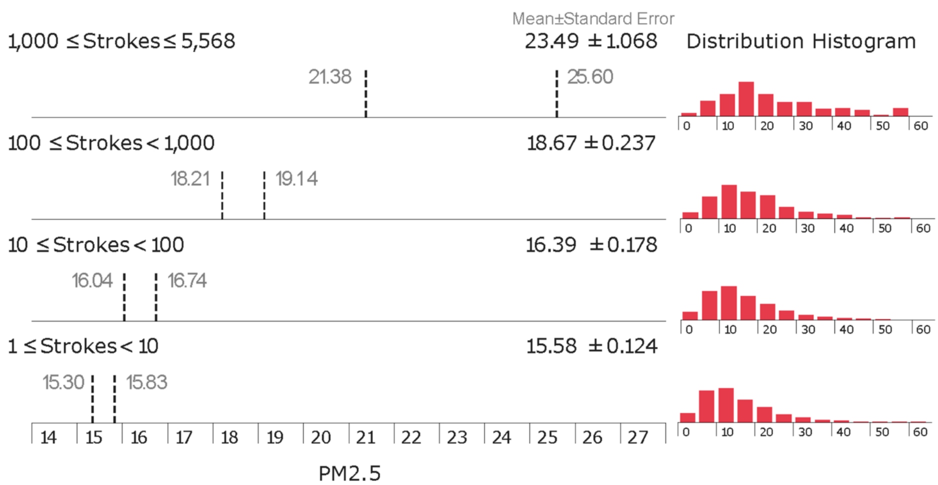

Fig. 4 Distribution of PM2.5 mean values +/- standard error and 95% confidence interval ranges across TE stroke count categories. Bar charts of the TE distribution in each stroke category are illustrated

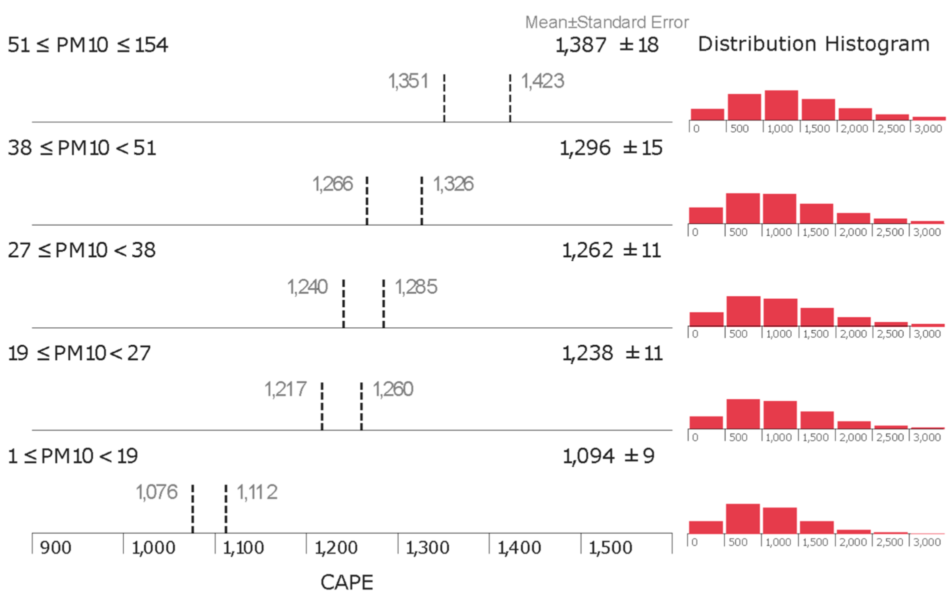

Fig. 5 Distribution of CAPE mean values +/- standard error and 95% confidence interval ranges across PM10 quantiles (25th, 50th, 75th, 90th). Bar charts of the TE distribution in each PM10 quantile are illustrated

than 2,000 J kg^{-1} initiating in environments with PM10 less than the 25th quantile (< 19 μg m^{-3}). The increase in TEs occurring in higher CAPE and PM10 environments is apparent in the rightward shift of the distribution bar graphs (Fig. 5). The spatial distribution of TEs initiating in both PM10 and CAPE environments above the 90th percentile shows that many of these events initiate and progress along the urban landcover boundary, possibly due to localized convergence, and then propagate parallel to the transport wind (Fig. 6; Westcott 1995; Stallins and Rose 2008; Bentley et al., 2021).

When dividing the PM10 90th quantile into two categories, separating by the 95th quantile (59 μg m^{-3}), evidence of aerosol radiative effects in stabilizing the atmosphere are apparent. There exists a statistically significant difference in the mean, median, and distribution in a decrease in CAPE, from sample means of 1,451 J kg^{-1} to 1,320 J kg^{-1}, for TEs initiating in PM10 environments below and above the 95th quantile, respectively. Therefore, it appears that for the BMR, it requires a higher concentration of PM10 (approximately 59 μg m^{-3}) versus PM2.5 (approximately 21 μg m^{-3}) aerosols to suppress thermodynamic instability and lower thunderstorm intensity (Figs. 3 and 5).

There exists a statistically significant, positive relationship in the mean, median, and distribution between TE

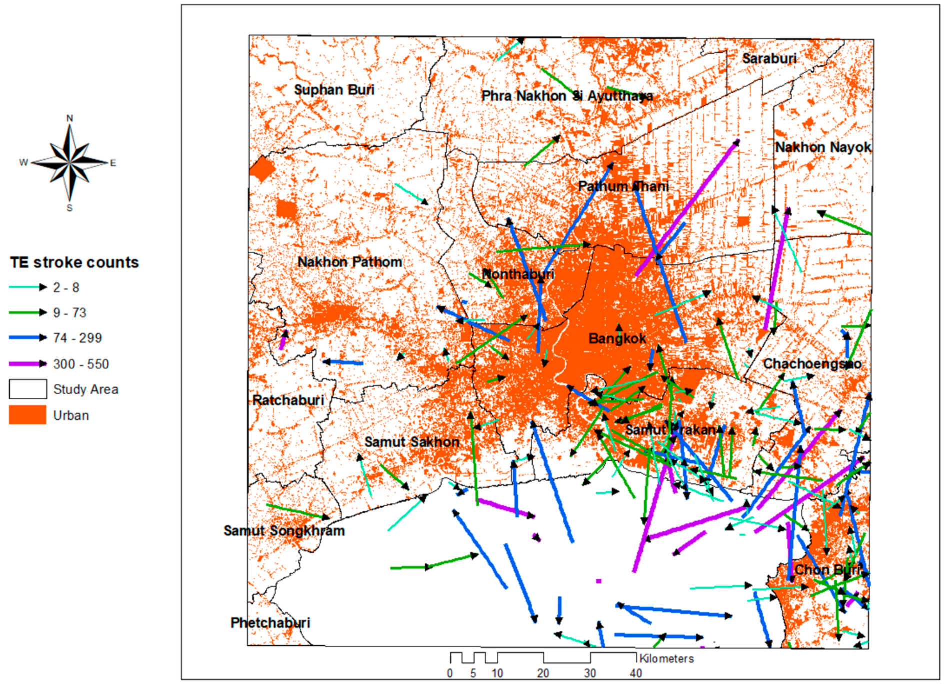

Fig. 6 Starting and ending coordinates plotted for 252 TEs initiating in environments with PM10 and CAPE greater than the 90th quantile. Urban land cover from the 2019–2023 reclassified land use from the Land Development Department, the Ministry for Agriculture and Cooperatives, Thailand is denoted

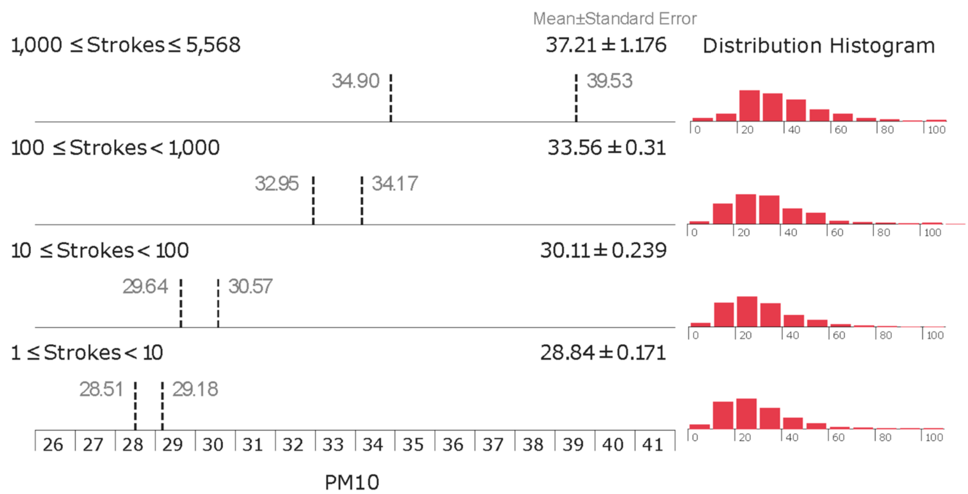

Fig. 7 Distribution of PM10 mean values +/- standard error and 95% confidence interval ranges across TE stroke count categories. Bar charts of the TE distribution in each stroke category are illustrated

strokes and PM10 concentration (Fig. 7). For TEs with greater than 1,000 strokes (912 events), the mean PM10 concentration is 37 µg m^{-3}, slightly less than the 75th quantile (Fig. 7; Table 1). Nearly 20% of TEs (43 of 217 TEs) with greater than 1,000 strokes initiated in PM10 environments of greater than 50 µg m^{-3} versus 9% of TEs (711 of 8,355) with less than 10 strokes. Although the variance in the standard error enlarges with increasing stroke counts, the PM10 concentration is significantly higher in TEs containing at least 100 strokes, supporting the role of aerosol concentration in promoting the non-inductive charge process (Fig. 7; Sun et al. 2023).

Evidence suggests, AOD is a useful measure to quantify the combined effects of aerosol concentrations on thunderstorms regardless of particle size (Wang et al. 2018; Sun et al. 2023; Bentley et al. 2024). There is a significant boomerang effect evident across AOD quantiles with respect to the CAPE distribution (Fig. 8). In BMR TE environments, CAPE is maximized in environments with AOD between the 50th and 75th quantile (0.34 to 0.54; Fig. 8). When examining the spatial distribution of high stroke TEs (90th quantile; >299 strokes) initiating between the 50th and 75th quantile of AOD, there is considerable initiation and tracking of events over the

Fig. 8 Distribution of CAPE mean values +/- standard error and 95% confidence interval ranges across AOD quantiles (25th, 50th, 75th, 90th). Bar charts of the TE distribution in each AOD quantile are illustrated

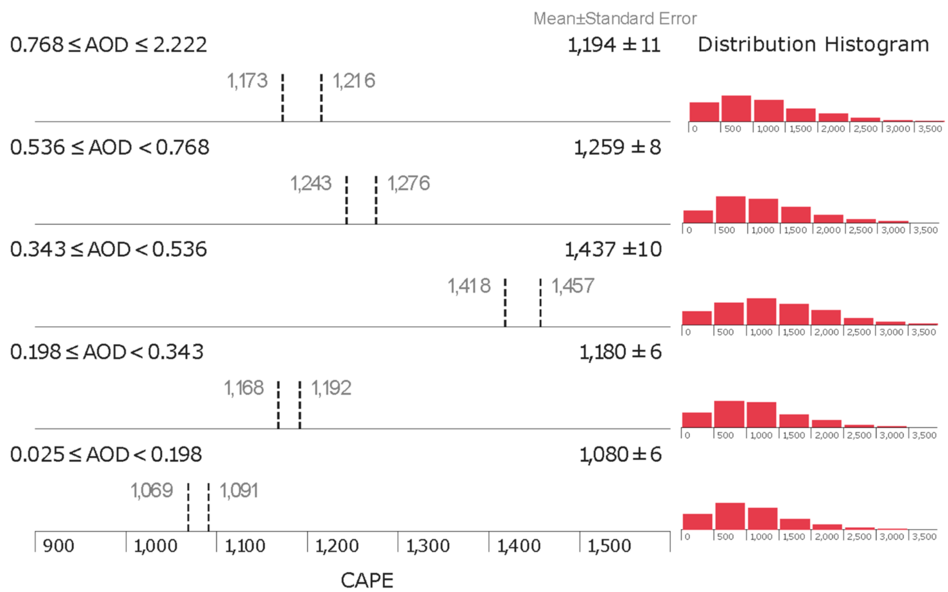

Fig. 9 Starting and ending coordinates plotted for 291 TEs initiating in environments with AOD in the 50-75th quantile and stroke counts greater than the 90th quantile. Urban land cover from the 2019–2023 reclassified land use from the Land Development Department, the Ministry for Agriculture and Cooperatives, Thailand is denoted

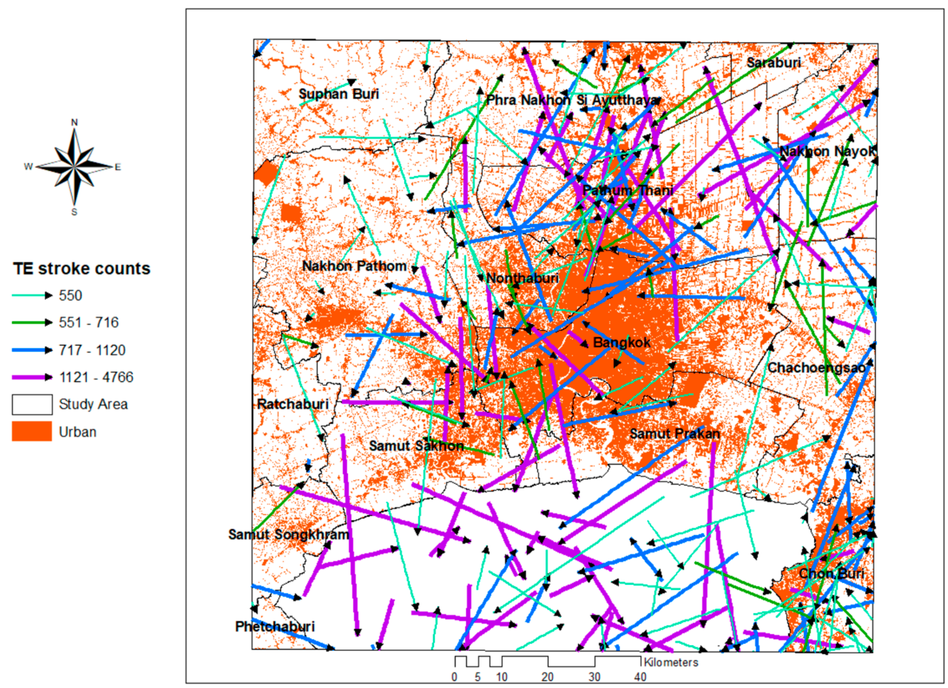

Bangkok urban core with a cluster of TEs initiating and progressing along the northern portion of the urban area (Fig. 9). Several of the largest TEs, in terms of stroke count, initiate along the edge of the urban/non-urban landcover and propagate with the mean steering winds (Fig. 9). Evidence suggests, the UHI acting with surface roughness disrupts airflow over the city and creates localized convergence zones along the urban/non-urban interface (Westcott 1995; Stallins and Rose 2008). Evidence suggests, localized forcing along the northern edge of the urban land cover can be a trigger for convection given other favorable environmental factors (Fig. 9). There also exists a statistically significant, positive relationship in the mean, median, and distribution between stroke counts and AOD for BMR TEs (Fig. 10). 10% of TEs producing greater than 1,000 strokes (88 of 866 TEs) and 7% of TEs producing less than 10 strokes (1,655 of 23,044 TEs) initiate in environments with AOD greater than 1.0.

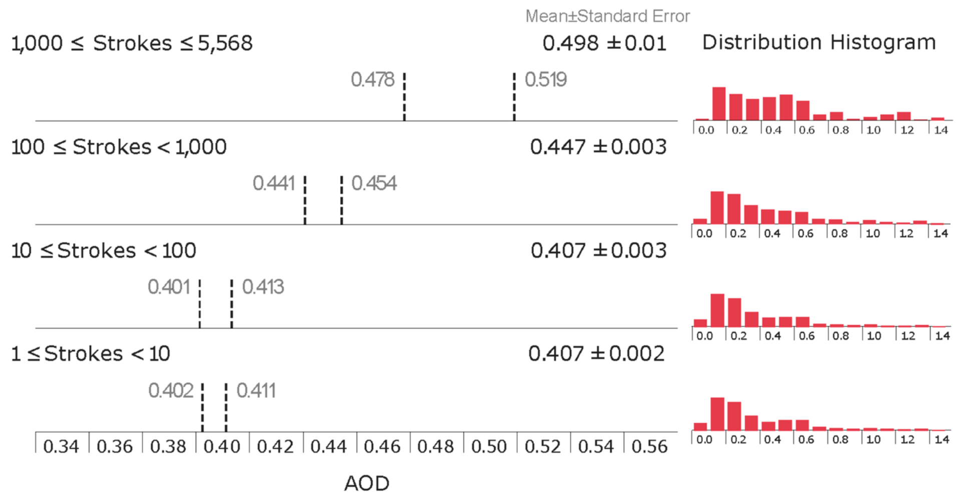

Fig. 10 Distribution of AOD mean values +/- standard error and 95% confidence interval ranges across TE stroke count categories. Bar charts of the AOD distribution in each stroke category are denoted

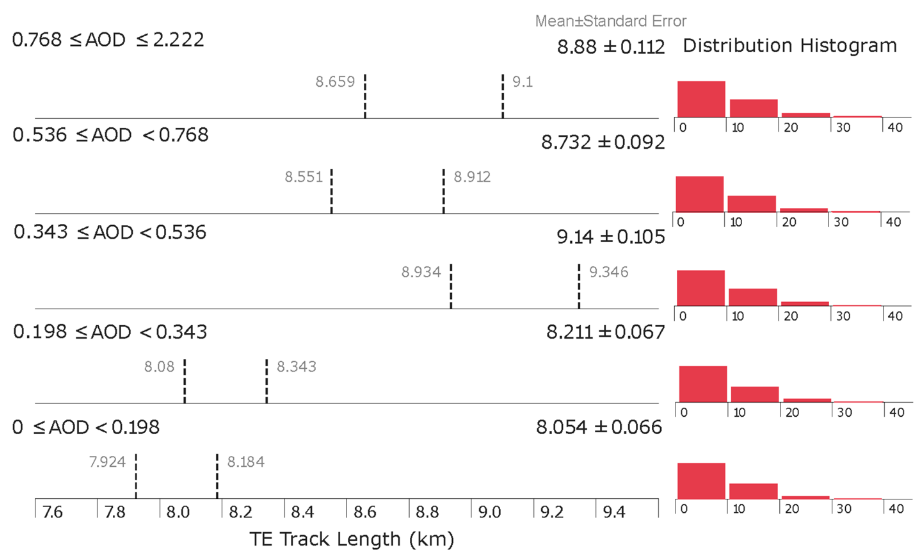

Fig. 11 Distribution of TE track length mean values +/- standard error and 95% confidence interval ranges across AOD quantiles (25th, 50th, 75th, 90th). Bar charts of the track length distribution in each AOD category are denoted

In contrast, TE track length is maximized in AOD environments between the 50th and 75th quantile, similar to CAPE (Figs. 8 and 10). Figure 11 shows that TE track lengths are reduced when AOD exceeds the 75th quantile (0.536). TEs initiating in the 90th quantile of AOD and CAPE are spatially located along the periphery of urban landcover and focused in the southwestern portions of Bangkok urban area, a region of land surface temperature increases due to rapid urbanization (Bentley et al. 2020; Fig. 12).

4.1 Covariation of Thermodynamic-Aerosol Environments

Further interrogation of BMR TEs consisted of visualizing the covariation of three variables across quantiles. Evidence suggests that PM2.5 increases strokes in TEs up to the 50 to 75th quantile and across all CAPE quantiles (14 to 21 μg m^{-3}; Fig. 13). The stroke augmentation is especially evident in CAPE environments greater than 2,172 J kg^{-1} (> 90% quantile; Fig. 13). TE environments with PM2.5 greater than the 75th quantile (21 μg m^{-3}) appear to lower stroke counts especially in the presence of higher instability (Figs. 3 and 13).

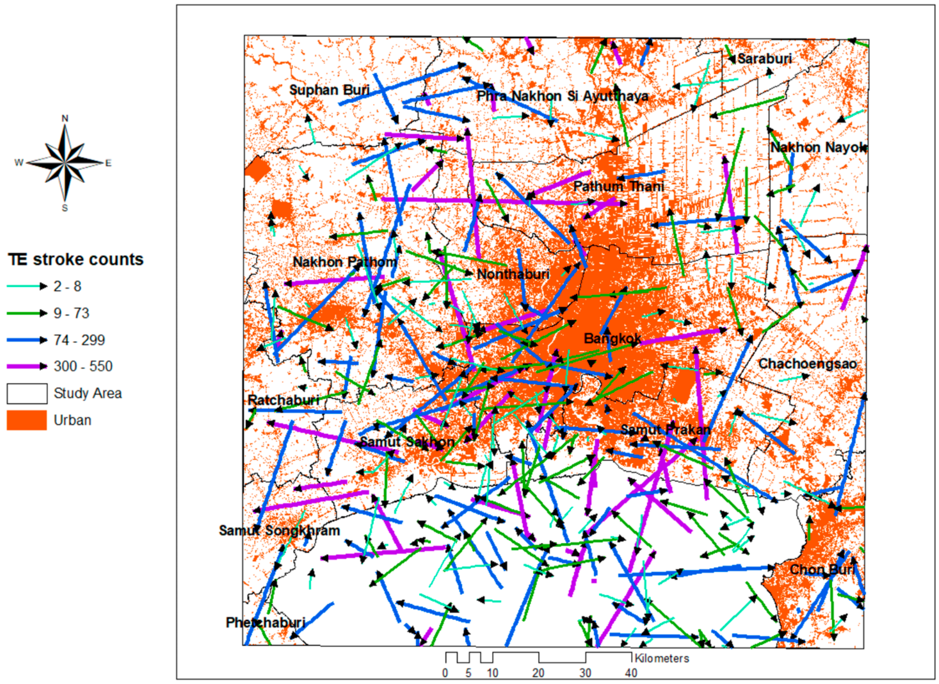

Fig. 12 Starting and ending coordinates plotted for 611 TEs initiating in environments with AOD and CAPE greater than the 90th quantile. Urban land cover from the 2019–2023 reclassified land use from the Land Development Department, the Ministry for Agriculture and Cooperatives, Thailand is denoted

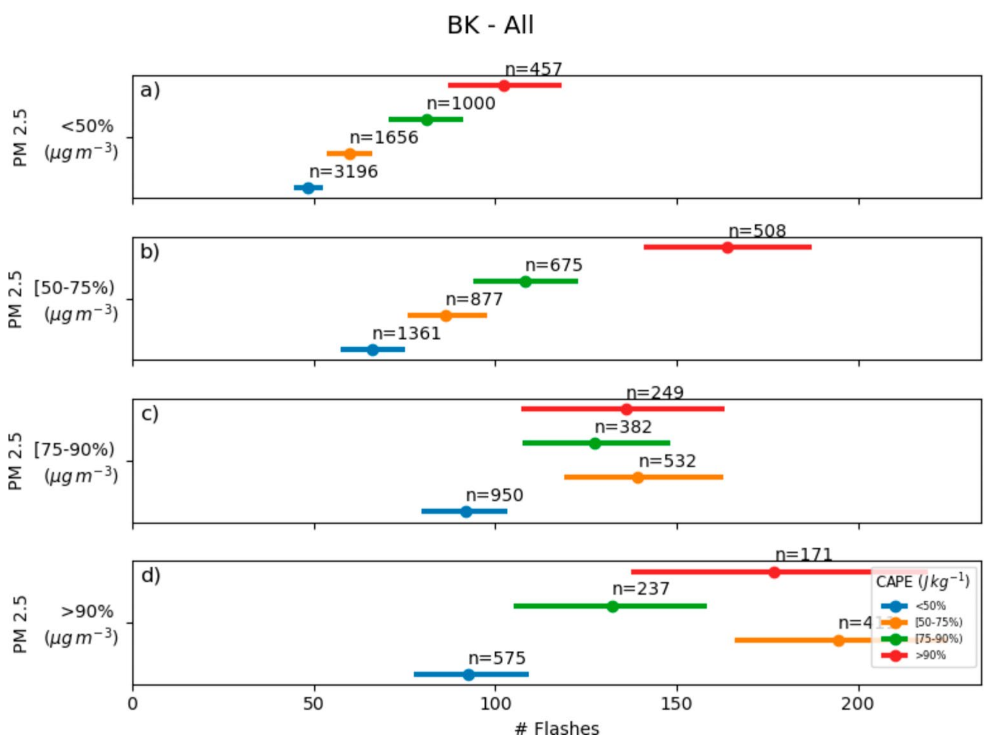

Fig. 13 Mean, sample size (n), and 95% confidence intervals for each PM2.5 quantile. (**a**) Total TE strokes by CAPE (J kg^{-1}) quantiles for thunderstorms in the BMR stratified by PM2.5 concentrations of the < 50% quantile. (**b**) same as a), except for PM2.5 concentrations of between 50 and 75% quantiles. (**c**) same as a), except for PM2.5 concentrations of between 75 and 90% quantiles. (**d**) same as a), except for PM2.5 concentrations of the > 90% quantile

TEs follow a similar progression when examining covariation of PM10, stroke counts, and CAPE, with one exception (Fig. 14). Curiously, TEs initiating in environments with PM10 in the 75 to 90th quantile (38 to 51 μg m^{-3}) and CAPE greater than the 90th quantile (2,172 J kg^{-1}) contain very high flash counts (mean of 300 strokes TE^{-1}; Fig. 14). These TEs appear to initiate near the urban/non-urban interface surrounding the BMR and then propagate over the urban core in a direction consistent with the mean steering winds (Fig. 15). TEs in other CAPE quantiles show slight increases in stroke counts until PM10 reaches the 75 to 90th percentile. However, stroke counts in TEs increase in environments with PM10 greater than the 90th quantile (51 μg m^{-3}) across all CAPE quantiles except the highest (> 90 quantile; 2,172 J kg^{-1}; Fig. 14). Evidence suggests that in environments of high

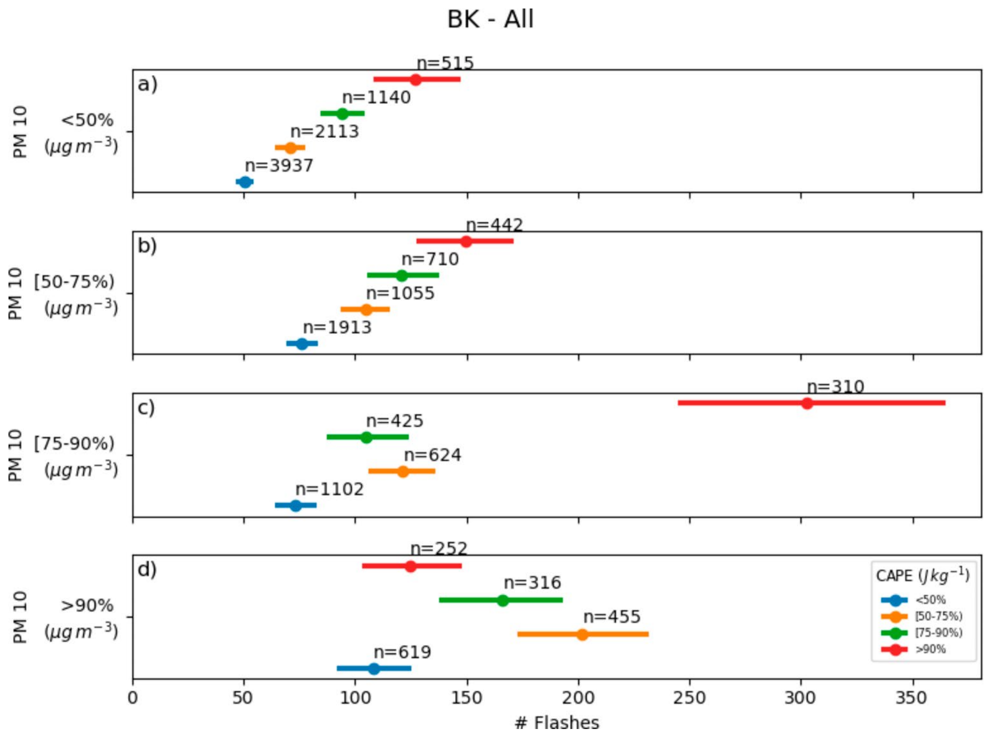

Fig. 14 Mean, sample size (n), and 95% confidence intervals for each PM10 quantile. (**a**) Total TE strokes by CAPE (J kg^{-1}) quantiles for thunderstorms in the BMR stratified by PM10 concentrations of the < 50% quantile. (**b**) same as a), except for PM10 concentrations of between 50 and 75% quantiles. (**c**) same as a), except for PM10 concentrations of between 75 and 90% quantiles. (**d**) same as a), except for PM10 concentrations of the > 90% quantile

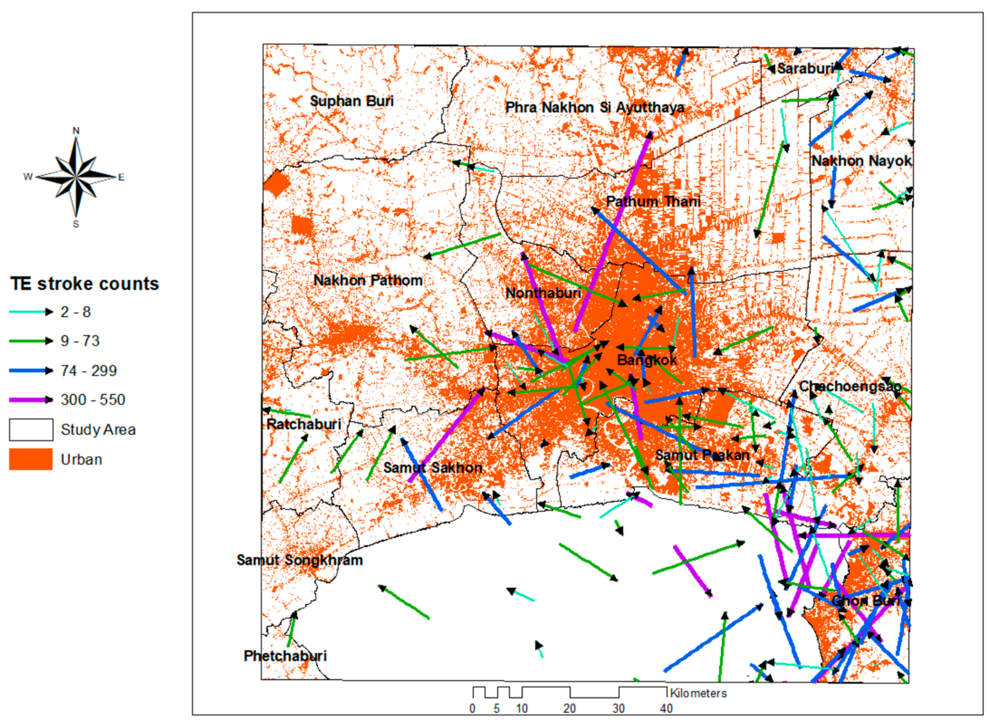

Fig. 15 Starting and ending coordinates plotted for 310 TEs initiating in environments with PM10 in the 75 to 90th quantile and CAPE greater than the 90th quantile. Urban land cover from the 2019–2023 reclassified land use from the Land Development Department, the Ministry for Agriculture and Cooperatives, Thailand is denoted

PM10 (> 51 μg m^{-3}), moderate instability (CAPE 1,087 to 2,172 J kg^{-1}) is most effective at generating increases in stroke counts in the BMR (Fig. 14). This corroborates with prior research findings examining urban thunderstorms surrounding Atlanta, GA (Bentley et al. 2012).

When examining the covariation of AOD with CAPE, evidence suggests significant suppression of TEs, based on stroke counts, does not occur until AOD becomes greater than the 90th quantile (0.77; Fig. 16). Curiously, in AOD and CAPE environments greater than the 90th quantile (0.77 and 2172 J kg^{-1}, respectively), stroke counts in TEs are maximized with a mean of nearly 400 strokes TE^{-1} (Fig. 16). The TEs forming in this environment appear to initiate along/near the urban/non-urban

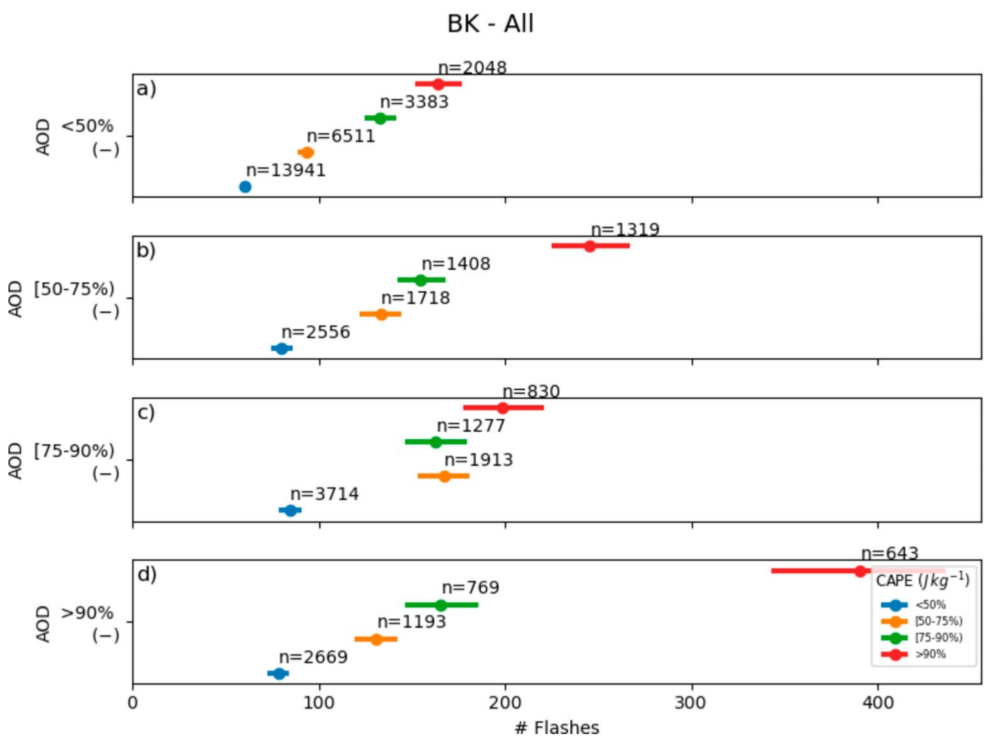

Fig. 16 Mean, sample size (n), and 95% confidence intervals for each AOD quantile. (**a**) Total TE strokes by CAPE (J kg^{-1}) quantiles for thunderstorms in the BMR stratified by AOD concentrations of the < 50% quantile. (**b**) same as a), except for AOD concentrations of between 50 and 75% quantiles. (**c**) same as a), except for AOD concentrations of between 75 and 90% quantiles. (**d**) same as a), except for AOD concentrations of the > 90% quantile

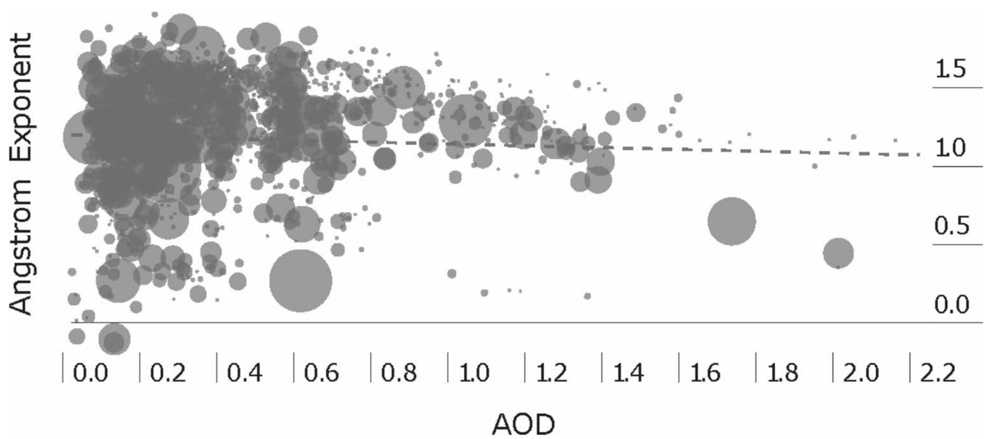

Fig. 17 Scatterplot with weighted markers of 440–675 nm Angstrom exponent by 500 nm AOD for 52,608 thunderstorms in the BMR

interface and appear to cluster on the western edge of the Bangkok urban region where significant increases in land surface temperatures due to urbanization has been identified between 2000 and 2019 (Fig. 12; Bentley et al. 2020).

There exists a statistically significant, negative relationship between AOD and AE for TE initiation environments (Fig. 17). As the TE initiation environment in the BMR becomes more polluted (AOD increases), the particle size of the aerosols also increases (AE decreases). Most TEs appear to initiate in environments with AOD < 0.4 and AE between 1.0 and 1.5 nm (Fig. 17). Evidence suggests there exists a particularly favorable relationship between AOD and AE in TE initiation environments within the BMR that is consistent with cities in the United States and South America (Morales Rodriguez et al. 2010; Bentley et al. 2024).

5 Conclusions

Prior research suggests that thunderstorms initiating in lower-CAPE environments may be more sensitive to aerosol effects (Sun et al. 2023). Likewise, numerical simulations have shown tropical environments may not be as supportive to aerosol effects on augmenting lightning and storm electrification due to a warmer mid-troposphere and limitations in graupel and rime ice formation (Van Weverberg et al. 2013; Sun et al. 2023). However, results from this investigation of TEs initiating in the BMR, a tropical environment, indicate that aerosol impacts are robust and, when examined in concert with instability, can significantly augment storm electrification and lightning formation.

Air pollution has become a significant issue in the BMR, as well as in many other Asian cities (Narita et al. 2019). A significant motivation for reducing anthropogenic particulates surrounds the impacts on human health; however, this research suggests that aerosols are also responsible for lightning augmentation in thunderstorms, another significant hazard to infrastructure and society (Wang et al. 2021). Recent findings suggest that reductions in anthropogenic aerosols in several Chinese cities have also reduced lightning densities mitigating the severity of this hazard. Traffic and biomass burning are responsible for over half of the anthropogenic air pollution in the BMR (Narita et al. 2019). Therefore, if sustained efforts are taken to reduce those sources of air pollution, evidence suggests that lightning frequencies in TEs within the BMR would also be lowered, leading to a reduction in the danger of this atmospheric hazard. Additionally, the positive relationship between CAPE and lightning appears significant across global thunderstorm environments. Since UHI enhancement increases thermodynamic instability (i.e., CAPE) and thunderstorm intensity, expanding the amount of per capita green space in the BMR would help to lessen thermodynamic instability and mitigate lightning frequency and thunderstorm intensity. Future research into the importance of thermodynamic-aerosol relationships in the BMR could include a numerical investigation examining the impact of changing land cover (i.e., green space) and improving air quality (i.e., lowering particulate matter) across thunderstorm environments and intensities.

Specific meteorological findings from this investigation include the following.

- Thermodynamic instability is positively correlated with stroke counts in TEs across all quantiles.
- PM2.5 and CAPE are positively related until PM2.5 reaches the 75th percentile (21 μg m^{-3}), then instability appears to be suppressed, possibly due to a shifting importance from microphysical to radiative effects of cloud aerosols. There exists a statistically significant, positive relationship between PM10 and CAPE across all PM10 quantiles. Evidence suggests that for the BMR, it requires a higher concentration of PM10 (approximately 59 μg m^{-3}) versus PM2.5 (approximately 21 μg m^{-3}) aerosols to suppress thermodynamic instability and thunderstorm intensity.
- TE environments with PM2.5 greater than the 75th quantile (21 μg m^{-3}) appear to lower stroke counts, especially in the presence of higher instability. The PM10 concentration is significantly higher in TEs containing at least 100 strokes, supporting the potential role of particulate matter concentration in promoting the non-inductive charge process. TEs initiating in environments with PM10 in the 75 to 90th quantile (38 to 51 μg m^{-3}) and CAPE greater than the 90th quantile (2,172 J kg^{-1}) contain very high flash counts (mean of 300 strokes TE^{-1}). Evidence suggests that in environments of high PM10 (> 51 μg m^{-3}), moderate instability (CAPE 1,087 to 2,172 J kg^{-1}) is most effective at generating increases in thunderstorm intensity.
- There is a significant boomerang effect evident across AOD quantiles with respect to the CAPE distribution. When examining the covariation of AOD with CAPE, evidence suggests significant suppression of TEs, based on stroke counts, does not occur until AOD becomes greater than the 90th quantile (0.77). In AOD and CAPE environments greater than the 90th quantile (0.77 and 2172 J kg^{-1}, respectively), stroke counts in TEs are maximized with a mean of nearly 400 strokes TE^{-1}.
- There exists a statistically significant, negative relationship between AOD and AE for TE initiation environments. As the TE initiation environment in the BMR becomes more polluted (AOD increases), the particle size of the aerosols also increases (AE decreases). Most TEs appear to initiate in a narrow window of AOD < 0.4 and AE between 1.0 and 1.5 nm.

Funding This research is funded by the Faculty of Liberal Arts Research Funds, Thammasat University, in the fiscal year of 2024 under the contract number 1/2567. Portions of this research are also supported by the National Science Foundation (Award #2104299; 2021).

Data availability Due to the GLD360's nature as a commercial dataset, we cannot share the underlying lightning data. ERA5 data used in this research is available at: https://cds.climate.copernicus.eu/cdsapp#!/dataset/reanalysis-era5-pressure-levels?tab=form. AERONET data were downloaded from: https://aeronet.gsfc.nasa.gov. Air pollution data were obtained from: https://www.pcd.go.th/

Declarations

Conflict of Interest On behalf of all authors, the corresponding author states that there is no conflict of interest.

References

Altaratz O, Koren I, Remer LA, Hirsch E (2014) Review: Cloud invigoration by aerosols—coupling between microphysics and dynamics. Atmos Res 140–141:38–60. https://doi.org/10.1016/j.atmosres.2014.01.009

Andreae MO, Rosenfeld D, Artaxo P et al (2004) Smoking rain clouds over the Amazon. Science 303:1337–1342. https://doi.org/10.1126/science.1092779

Arfanuzzaman Md, Dahiya B (2019) Sustainable urbanization in Southeast Asia and beyond: challenges of population growth, land use change, and environmental health. Growth Change 50:725–744. https://doi.org/10.1111/grow.12297

Arifwidodo SD, Tanaka T (2015) The Characteristics of Urban Heat Island in Bangkok, Thailand. Procedia - Social Behav Sci 195:423–428. https://doi.org/10.1016/j.sbspro.2015.06.484

Bentley ML, Stallins JA, Ashley WS (2012) Synoptic environments favourable for urban convection in Atlanta, Georgia: SYNOPTIC ENVIRONMENTS FAVOURABLE FOR URBAN CONVECTION. Int J Climatol 32:1287–1294. https://doi.org/10.1002/joc.2344

Bentley ML, Sae-Jung J, Kaminski S, Kesavawong P (2020) Documenting the evolution and expansion of surface urban heat in the Bangkok Metropolitan Region, 2000–2019. Asian Geogr 37:171–188. https://doi.org/10.1080/10225706.2020.1745251

Bentley ML, Sae-Jung J, Kaminski S, Terry CC (2021) A spatiotemporal analysis of lightning in the Bangkok Metropolitan Region. Asian Geogr 40:99–120. https://doi.org/10.1080/10225706.2021.2010579

Bentley M, Gerken T, Duan Z et al (2024) Toward untangling thunderstorm-aerosol relationships: an observational study of regions centered on Washington, DC and Kansas City, MO. Atmos Res 304:107402. https://doi.org/10.1016/j.atmosres.2024.107402

Carrió GG, Cotton WR (2011) Urban growth and aerosol effects on convection over Houston. Part II: dependence of aerosol effects on instability. Atmos Res 102:167–174. https://doi.org/10.1016/j.atmosres.2011.06.022

Craven JP, Brooks HE (2004) Baseline climatology of sounding derived parameters associated with deep moist convection. Natl Wea Dig 28:13–24. https://www.nssl.noaa.gov/users/brooks/public_html/papers/cravenbrooksnwa.pdf

Dewan A, Ongee ET, Rafiuddin M et al (2018) Lightning activity associated with precipitation and CAPE over Bangladesh: LIGHTNING IN BANGLADESH. Int J Climatol 38:1649–1660. https://doi.org/10.1002/joc.5286

Dewan A, Islam KMA, Enan ME et al (2024) Cloud-to-ground lightning in cities: Seasonal Variability and influential factors. Earth Syst Environ. https://doi.org/10.1007/s41748-024-00372-6

Ekman AML, Engström A, Söderberg A (2011) Impact of two-way aerosol–Cloud Interaction and changes in aerosol size distribution on simulated Aerosol-Induced Deep Convective Cloud sensitivity. J Atmos Sci 68:685–698. https://doi.org/10.1175/2010JAS3651.1

Fan J, Zhang R, Li G, Tao W-K (2007) Effects of aerosols and relative humidity on cumulus clouds. J Geophys Res 112:D14204. https://doi.org/10.1029/2006JD008136

Fan J, Leung LR, Rosenfeld D et al (2013) Microphysical effects determine macrophysical response for aerosol impacts on deep convective clouds. Proc Natl Acad Sci USA 110. https://doi.org/10.1073/pnas.1316830110

Fuchs BR, Rutledge SA, Bruning EC et al (2015) Environmental controls on storm intensity and charge structure in multiple regions of the continental United States: STORM ENVIRONMENTAL CONTROLS. J Geophys Res Atmos 120:6575–6596. https://doi.org/10.1002/2015JD023271

Green M, Kondragunta S, Ciren P, Xu C (2009) Comparison of GOES and MODIS Aerosol Optical depth (AOD) to Aerosol Robotic Network (AERONET) AOD and IMPROVE PM 2.5 Mass at Bondville, Illinois. J Air Waste Manag Assoc 59:1082–1091. https://doi.org/10.3155/1047-3289.59.9.1082

Guo J, Liu H, Li Z et al (2018) Aerosol-induced changes in the vertical structure of precipitation: a perspective of TRMM precipitation radar. Atmos Chem Phys 18:13329–13343. https://doi.org/10.5194/acp-18-13329-2018

Hersbach H, Bell B, Berrisford P et al (2020) The ERA5 global reanalysis. QJR Meteorol Soc 146:1999–2049. https://doi.org/10.1002/qj.3803

Holle RL, Murphy MJ (2017) Lightning over three large Tropical Lakes and the Strait of Malacca: exploratory analyses. Mon Weather Rev 145:4559–4573. https://doi.org/10.1175/MWR-D-17-0010.1

Holle RL, Said R, Scott M (2017) Global lightning variations: Lightning for each continent through the year. Met Tech Intl 1039–1240

Huang T, Zhu Y, Rosenfeld D et al (2022) Regime-Dependent impacts of Aerosol Particles and updrafts on the Cloud condensation nuclei and the enhanced warm rain suppression: evidence from Synergistic Satellite and LiDAR observations. Geophys Res Lett 49:e2021GL097315. https://doi.org/10.1029/2021GL097315

James G, Witten D, Hastie T, Tibshirani R (2017) An introduction to statistical learning: with applications in R, corrected at 8th printing. Springer, New York Heidelberg Dordrecht London

Karson M Handbook of Methods of Applied Statistics. Volume I: Techniques of Computation Descriptive Methods, and Statistical Inference. Volume II: Planning of Surveys and Experiments. I. M., Chakravarti RG, Laha, Roy J (1968) New York, John Wiley; 1967, $9.00. Journal of the American Statistical Association 63:1047–1049. https://doi.org/10.1080/01621459.1968.11009335

Khain A, Rosenfeld D, Pokrovsky A (2005) Aerosol impact on the dynamics and microphysics of deep convective clouds. Quart J Royal Meteoro Soc 131:2639–2663. https://doi.org/10.1256/qj.04.62

Khain AP, BenMoshe N, Pokrovsky A (2008) Factors determining the impact of Aerosols on Surface Precipitation from clouds: an attempt at classification. J Atmos Sci 65:1721–1748. https://doi.org/10.1175/2007JAS2515.1

Konwar M, Maheskumar RS, Kulkarni JR et al (2012) Aerosol control on depth of warm rain in convective clouds. J Geophys Res 117:2012JD017585. https://doi.org/10.1029/2012JD017585

Koren I, Martins JV, Remer LA, Afargan H (2008) Smoke invigoration Versus Inhibition of clouds over the Amazon. Science 321:946–949. https://doi.org/10.1126/science.1159185

Kottek M, Grieser J, Beck C et al (2006) World Map of the Köppen-Geiger climate classification updated. metz 15:259–263. https://doi.org/10.1127/0941-2948/2006/0130

Kruskal WH, Wallis WA (1952) Use of ranks in One-Criterion Variance Analysis. J Am Stat Assoc 47:583–621. https://doi.org/10.1080/01621459.1952.10483441

Li B, Yuan H, Feng N, Tao S (2009) Comparing MODIS and AERONET aerosol optical depth over China. Int J Remote Sens 30:6519–6529. https://doi.org/10.1080/01431160903111069

Li Z, Rosenfeld D, Fan J (2017) Aerosols and their impact on Radiation, clouds, Precipitation, and severe Weather events. In: Oxford Research Encyclopedia of Environmental Science. Oxford University Press

MacGorman DR, Rust WD (1998) The electrical nature of storms. Oxford University Press, New York Oxford

Mallick S, Rakov VA, Ngin T et al (2014) Evaluation of the GLD360 performance characteristics using rocket-and-wire triggered lightning data. Geophys Res Lett 41:3636–3642. https://doi.org/10.1002/2014GL059920

Miller ME (1967) Forecasting afternoon mixing depths and transport wind speeds. Mon Wea Rev 95:35–44. https://doi.org/10.1175/1520-0493(1967)095%3C0035:FAMDAT%3E2.3.CO;2

Morales Rodriguez CA, da Rocha RP, Bombardi R (2010) On the development of summer thunderstorms in the city of São Paulo: Mean meteorological characteristics and pollution effect. Atmos Res 96:477–488. https://doi.org/10.1016/j.atmosres.2010.02.007

Murugavel P, Pawar SD, Gopalakrishan V (2014) Climatology of lightning over Indian region and its relationship with convective available potential energy. Int J Climatol 34:3179–3187. https://doi.org/10.1002/joc.3901

Naccarato KP, Pinto O, Pinto IRCA (2003) Evidence of thermal and aerosol effects on the cloud-to-ground lightning density and polarity over large urban areas of Southeastern Brazil: urban effects on lightning. Geophys Res Lett 30. https://doi.org/10.1029/2003GL017496

Narita D, Oanh N, Sato K et al (2019) Pollution characteristics and policy actions on fine particulate matter in a growing Asian Economy: the case of Bangkok Metropolitan Region. Atmosphere 10:227. https://doi.org/10.3390/atmos10050227

Oke TR (1982) The energetic basis of the urban heat island. Quart J Royal Meteoro Soc 108:1–24. https://doi.org/10.1002/qj.49710845502

Pawar SD, Lal DM, Murugavel P (2012) Lightning characteristics over central India during Indian summer monsoon. Atmos Res 106:44–49. https://doi.org/10.1016/j.atmosres.2011.11.007

Pérez-Invernón FJ, Gordillo-Vázquez FJ, Huntrieser H, Jöckel P (2023) Variation of lightning-ignited wildfire patterns under climate change. Nat Commun 14:739. https://doi.org/10.1038/s41467-023-36500-5

Poelman DR, Schulz W, Vergeiner C (2013) Performance characteristics of distinct lightning detection Networks Covering Belgium. J Atmos Ocean Technol 30:942–951. https://doi.org/10.1175/JTECH-D-12-00162.1

Reynolds SE, Brook M, Gourley MF (1957) Thunderstorm charge separation. J Meteor 14:426–436. https://doi.org/10.1175/1520-0469(1957)014%3C0426:TCS%3E2.0.CO;2

Rosenfeld D, Lensky IM (1998) Satellite–based insights into precipitation formation processes in Continental and Maritime Convective clouds. Bull Amer Meteor Soc 79:2457–2476. https://doi.org/10.1175/1520-0477(1998)079%3C2457:SBIIPF%3E2.0.CO;2

Rosenfeld D, Lahav R, Khain A, Pinsky M (2002) The role of Sea Spray in Cleansing Air Pollution over Ocean via Cloud processes. Science 297:1667–1670. https://doi.org/10.1126/science.1073869

Rosenfeld D, Lohmann U, Raga GB et al (2008) Flood or Drought: how do aerosols affect precipitation? Science 321:1309–1313. https://doi.org/10.1126/science.1160606

Rosenfeld D, Andreae MO, Asmi A et al (2014) Global observations of aerosol-cloud-precipitation-climate interactions: aerosol-cloud-climate interactions. Rev Geophys 52:750–808. https://doi.org/10.1002/2013RG000441

Rosenfeld D, Zheng Y, Hashimshoni E et al (2016) Satellite retrieval of cloud condensation nuclei concentrations by using clouds as CCN chambers. Proc Natl Acad Sci USA 113:5828–5834. https://doi.org/10.1073/pnas.1514044113

Sae-Jung J, Bentley M, Duan Z, Szakal E (2024) Developing an urban thunderstorm climatology for the Bangkok Metropolitan Region. Singap J Trop Geog. https://doi.org/10.1111/sjtg.12552

Said RK, Murphy MJ (2016) GLD360 upgrade: performance analysis and applications. Vaisala, Inc., San Francisco, CA

Said RK, Inan US, Cummins KL (2010) Long-range lightning geolocation using a VLF radio atmospheric waveform bank. J Geophys Res 115:D23108. https://doi.org/10.1029/2010JD013863

Schmid PE, Niyogi D (2017) Modeling Urban Precipitation modification by spatially heterogeneous aerosols. J App Meteor Clim 56:2141–2153. https://doi.org/10.1175/JAMC-D-16-0320.1

Seity Y, Soula S, Tabary P, Scialom G (2003) The convective storm system during IOP 2a of MAP: cloud-to-ground lightning flash production in relation to dynamics and microphysics. Quart J Royal Meteoro Soc 129:523–542. https://doi.org/10.1256/qj.02.03

Small C, Sousa D, Yetman G et al (2018) Decades of urban growth and development on the Asian megadeltas. Glob Planet Change 165:62–89. https://doi.org/10.1016/j.gloplacha.2018.03.005

Stallins JA, Rose LS (2008) Urban lightning: current research, methods, and the geographical perspective. Geogr Compass 2:620–639. https://doi.org/10.1111/j.1749-8198.2008.00110.x

Stallins J, Bentley M, Rose L (2006) Cloud-to-ground flash patterns for Atlanta, Georgia (USA) from 1992 to 2003. Clim Res 30:99–112. https://doi.org/10.3354/cr030099

Stallins JA, Carpenter J, Bentley ML et al (2013) Weekend–weekday aerosols and geographic variability in cloud-to-ground lightning for the urban region of Atlanta, Georgia, USA. Reg Environ Change 13:137–151. https://doi.org/10.1007/s10113-012-0327-0

Steiger SM, Orville RE (2003) Cloud-to-ground lightning enhancement over Southern Louisiana. Geophys Res Lett 30. https://doi.org/10.1029/2003GL017923. 2003GL017923

Sun M, Qie X, Mansell ER et al (2023) Aerosol impacts on Storm Electrification and Lightning discharges under different thermodynamic environments. JGR Atmos 128. https://doi.org/10.1029/2022JD037450. e2022JD037450

Tao W, Li X, Khain A et al (2007) Role of atmospheric aerosol concentration on deep convective precipitation: cloud-resolving model simulations. J Geophys Res 112:2007JD008728. https://doi.org/10.1029/2007JD008728

Tao W, Chen J, Li Z et al (2012) Impact of aerosols on convective clouds and precipitation. Rev Geophys 50. https://doi.org/10.1029/2011RG000369. 2011RG000369

Thompson RL, Edwards R, Hart JA et al (2003) Close Proximity soundings within Supercell environments obtained from the Rapid Update cycle. Wea Forecast 18:1243–1261. https://doi.org/10.1175/1520-0434(2003)018%3C1243:CPSWSE%3E2.0.CO;2

van den Heever SC, Cotton WR (2007) Urban Aerosol Impacts on Downwind Convective storms. J Appl Meteorol Climatology 46:828–850. https://doi.org/10.1175/JAM2492.1

van den Heever SC, Carrió GG, Cotton WR et al (2006) Impacts of Nucleating Aerosol on Florida Storms. Part I: Mesoscale simulations. J Atmos Sci 63:1752–1775. https://doi.org/10.1175/JAS3713.1

van den Heever SC, Stephens GL, Wood NB (2011) Aerosol Indirect effects on Tropical Convection characteristics under conditions of radiative–convective equilibrium. J Atmos Sci 68:699–718. https://doi.org/10.1175/2010JAS3603.1

van Weverberg K, Vogelmann AM, Lin W et al (2013) The role of Cloud Microphysics parameterization in the Simulation of Mesoscale Convective System clouds and Precipitation in the Tropical Western Pacific. J Atmos Sci 70:1104–1128. https://doi.org/10.1175/JAS-D-12-0104.1

Voogt JA, Oke TR (2003) Thermal remote sensing of urban climates. Remote Sens Environ 86:370–384. https://doi.org/10.1016/S0034-4257(03)00079-8

Wang J, Van Den Heever SC, Reid JS (2009) A conceptual model for the link between central American biomass burning aerosols and severe weather over the south-central United States. Environ Res Lett 4:015003. https://doi.org/10.1088/1748-9326/4/1/015003

Wang Y, Wan Q, Meng W et al (2011) Long-term impacts of aerosols on precipitation and lightning over the Pearl River Delta megacity area in China. Atmos Chem Phys 11:12421–12436. https://doi.org/10.5194/acp-11-12421-2011

Wang Q, Li Z, Guo J et al (2018) The climate impact of aerosols on the lightning flash rate: is it detectable from long-term measurements? Atmos Chem Phys 18:12797–12816. https://doi.org/10.5194/acp-18-12797-2018

Wang H, Shi Z, Wang X et al (2021) Cloud-to-ground lightning response to Aerosol over Air-Polluted Urban areas in China. Remote Sens 13:2600. https://doi.org/10.3390/rs13132600

Wang Y, Wang Y, Song X et al (2023) The impact of particulate pollution control on aerosol hygroscopicity and CCN activity in North China. Environ Res Lett 18:074028. https://doi.org/10.1088/1748-9326/acde91

Westcott NE (1995) Summertime cloud-to-ground lightning activity around major midwestern urban areas. J Appl Meteorol 34:1633–1642. https://doi.org/10.1175/1520-0450-34.7.1633

Williams E, Rosenfeld D, Madden N et al (2002) Contrasting convective regimes over the Amazon: implications for cloud electrification. J Geophys Res 107. https://doi.org/10.1029/2001JD000380

Williams E, Chan T, Boccippio D (2004) Islands as miniature continents: another look at the land-ocean lightning contrast. J Geophys Res 109:2003JD003833. https://doi.org/10.1029/2003JD003833

Williams E, Mushtak V, Rosenfeld D et al (2005) Thermodynamic conditions favorable to superlative thunderstorm updraft, mixed phase microphysics and lightning flash rate. Atmos Res 76:288–306. https://doi.org/10.1016/j.atmosres.2004.11.009

Yair Y (2018) Lightning hazards to human societies in a changing climate. Environ Res Lett 13:123002. https://doi.org/10.1088/1748-9326/aaea86

Yair YY, Lynn BH, Korzets M, Jaffe M (2022) The Weekend Effect in Lightning Activity during Winter thunderstorms over the Tel-Aviv, Israel, Metropolitan Area. Atmosphere 13:1570. https://doi.org/10.3390/atmos13101570

Zhu Y, Rosenfeld D, Yu X et al (2014) Satellite retrieval of convective cloud base temperature based on the NPP/VIIRS Imager. Geophys Res Lett 41:1308–1313. https://doi.org/10.1002/2013GL058970

Zhu Y, Rosenfeld D, Yu X, Li Z (2015) Separating aerosol microphysical effects and satellite measurement artifacts of the relationships between warm rain onset height and aerosol optical depth. JGR Atmos 120:7726–7736. https://doi.org/10.1002/2015JD023547

Mace Bentley is a geographer who has teaching and research interests in weather-societal interactions, urban meteorology/climatology, and severe storms. This interdisciplinary research focuses on issues surrounding human-land-atmosphere interactions and aims to untangle their complex, critical relationships.